Journal of Intelligent Systems and Internet of Things
Vol. 16, No. 02, PP. 68-81, 2025
DOI: https://doi.org/10.54216/JISIoT.160206

Leveraging Quantum Neural Networks with Deep Learning Based Edge Detection Model for Breast Cancer Screening using Digital Mammograms

S. Abdel-Khalek[1,2,*]
[1]Department of Mathematics and Statistics, College of Science, Taif University, P.O. Box 11099, Taif 21944, Saudi Arabia
[2]Department of Mathematics, Faculty of Science, Sohag University, 82524 Sohag, Egypt
Email: sayedquantum@yahoo.co.uk

Abstract
Breast cancer (BC) is one of the most common invasive cancers, which cause thousands of women's deaths globally. Therefore, prompt detection is a cure for reducing the rate of death. Therefore, screening of BC in its initial phase is of utmost vital. Physically segmenting breast lesion imaging appears a time-consuming and expensive pursuit for radiologists. Hence, the adoption of automatic analytic techniques becomes vital, directing to exactly segment lesions of the breast and mitigate the associated tasks. The segmentation of malignant areas is an essential procedure in the complete inspection of breast image data. To achieve the segmentation and recognition of BC, numerous computer-aided diagnosis (CAD) techniques were presented for the investigation of mammogram imaging. The CAD models are employed to mainly analyze the disorder and provide the best treatment. Currently, deep learning (DL) techniques are superior and provide promising results in the early recognition of BC. In this paper, we design a Leveraging Quantum Algorithms for Edge Detection in Mammograms to Improve Breast Cancer Screening (LQAEDM-IBCS) model. The main intention of the LQAEDM-IBCS is to provide an accurate and effective technique for the detection and segmentation process of breast cancer using advanced algorithms. Initially, the image pre-processing stage applies the adaptive bilateral filtering (ABF) method to eliminate the unwanted noise in input image data. Next, the segmentation process is implemented by the Otsu threshold method for edge detection. To improve the segmentation performance, the parameter tuning process is performed through the quantum spotted hyena optimizer (QSHO) algorithm. Besides, the proposed LQAEDM-IBCS technique designs the DenseNet-121 method for the extraction of feature procedure. Eventually, the quantum neural network (QNN) method has been deployed for the BC classification process. The simulating validation of the LQAEDM-IBCS system is verified on a benchmark image database and the outcomes are dignified under numerous measures. The experimental outcome emphasized the enlargement of the LQAEDM-IBCS approach in the BC diagnosis process.

Received: October 18, 2024 Revised: February 07, 2025 Accepted: March 02, 2025

Keywords: Breast Cancer; Quantum Algorithms; Edge Detection; Mammograms; Image Pre-processing; Otsu Threshold

1. Introduction

Breast cancer (BC) typically begins with the formation of a small tumor due to the accumulation of abnormal cells or the deposition of calcium in breast tissue [1]. During cancer progression, cells grow uncontrollably. Notably, BC is one of the most common tumors in women and is the 2nd leading cause of cancer-related mortality after lung cancer. Therefore, the survivability for greater than 5 years is so low, that a variability of 10–40% is because the healthcare system's capability is highly restricted [2]. Nevertheless, if the disorder is early, identified and the patients receive proper treatment; their chances of living are 80% more than five years. Recognition of BC and its analysis at initial periods results the treatment success and completed patient recovery [3]. Mammography

scanning is a major efficient method for identifying cancer's earlier symptoms appearance. It is used to get what is inside the breast problem via X-ray imaging with a small dose of ionizing radiation. Due to the quality of limited of the attained images, cancers are not effectively differentiated from images and eyes [4]. Distinguishing both malignant and benign tumors is also a difficult task as the anomalous parts are complicated, and so mammogram explanation is a tough job for radiologists [5].

However, Computer-aided diagnosis (CAD) systems based on medicinal screening may be apposite and that can minimize the authority's efforts [6]. CAD analysis plays a significant role in BC diagnosis and should be efficiently employed in the science of biomedical. The prevalent CAD is based on health check-ups such as Magnetic Resonance Imaging (MRI), mammogram, and ultrasound [7]. Mammograms are a reliable, low-dose, highly efficient and slow-invasive diagnosis technique for the basic ID of BC. CAD methods are automatic with mammograms growths the precision level of detection; the effective benefit accelerates the analyzing procedure and the health appliances retain [8]. Furthermore, some division processes proposed for helping radiologists in BC recognition face tasks with computational difficulty and normally require manual interventions. Addressing these tasks is vital for enhancing the efficacy and dependability of deep learning (DL) methods for BC segmentation [9]. In current years, the pervasive acceptance of DL procedures has led to significant gains in several areas with a plenitude of architectural forms. The DL technique has shown consistency and enhanced accuracy over many areas. Furthermore, DL has demonstrated its efficiency in the region of medical images, generally in the breast imaging analysis data and its applications have revealed promising outcomes [10].

This paper designs and develops a Leveraging Quantum Algorithms for Edge Detection in Mammograms to Improve Breast Cancer Screening (LQAEDM-IBCS) model. Initially, the image pre-processing stage applies the adaptive bilateral filtering (ABF) method to eliminate the unwanted noise in input image data. Next, the segmentation process is implemented by the Otsu threshold method for edge detection. To improve the segmentation performance, the parameter tuning process is performed through the quantum spotted hyena optimizer (QSHO) algorithm. Besides, the proposed LQAEDM-IBCS technique designs the DenseNet-121 method for the extraction of feature procedure. Eventually, the quantum neural network (QNN) method has been deployed for the BC classification process. The experimental outcome emphasized the enlargement of the LQAEDM-IBCS approach in the BC diagnosis process.

2. Related Works

Youssef et al. [11] present an innovative hybrid feature extraction method combining conventional and DL methodologies. The projected model creates the utilization of dual major models for feature extraction. The primary model creates edge and texture maps depending on the holistically nested edge detector, canny edge detector, and Gabor filter bank. Subsequently, the histogram of oriented gradients (HOG) is employed for extraction. Another model removes deep attributes from the breast images acquiring higher-level predictive data utilizing MobileNet and ResNet-50 pre-trained CNNs. The principal component analysis (PCA) is employed for reducing dimensionality. Olota et al. [12] present the Least Square SVM (LSSVM) to enhance the prediction and classification precision of breast thermography images employing enhanced hyper-parameters. Canny edge identification was implemented in the segmented output to restrict the number of filters and data. Ghafariasl et al. [13] employ DL and TL methodologies to remove and differentiate attributes from a collective database. The pre-processing stages include the removal of artifacts, image cropping, and improvement of divergence utilizing CLAHE. Data augmentation models, comprising the application of Gaussian blur and median are utilized for enhancing the sturdiness of techniques. There are 3 pre-trained systems namely VGG-19, ResNet-152V2, and ResNet-50 were modified particularly for mammography data.

In [14], an innovative unsupervised BC image classification method depends on multi-scale texture investigation, and a dynamic learning approach for mammograms is projected. Primarily, Tamura coarseness and gray-level co-occurrence matrices are employed to transfer images to multi-scale texture vector features. Bilal et al. [15] present a hybrid model to improve BC classification precision. The projected Q-BGWO-SQSVM model employs an upgraded quantum-inspired binary GWO and integrates with SqueezeNet and SVM to demonstrate cutting-edge performance. Complex bypass mechanisms and SqueezeNet's fire modules remove diverse features from mammography images.

Singh and Alam [16] project an effective hybrid model for the identification and localization of distrustful mass regions. The presented hybrid method is advanced by incorporating an effective pixel-based lower-level pre-processing model with Faster R-CNN. Furthermore, an effective mass recognition model was projected which comprises the usage of Faster R-CNN and pixel-based lower-level pre-processing models. Taheri and Rahbar [17] employ pre-trained systems and apply a TL approach. In this model, the AlexNet methodology is employed for extracting features from ultrasound images. Therefore, the presented model attempts to differentiate the feature space removed from the neural method utilizing hashing layers combined with Siamese structure. Subsequently

choosing effectual attributes and decreasing the dimension of vector features by employing the RF classifier and Boruta- SHAP method is utilized for the final classification.

3. The Proposed Methodology

In this study, we design an LQAEDM-IBCS model. The main objective of the LQAEDM-IBCS is to provide an accurate and effective performance for the detection and segmentation process of BC using advanced algorithms. It contains five various stages involving image pre-processing, segmentation, parameter optimization, feature extractor, and BC classification. Fig. 1 represents the entire flow of the LQAEDM-IBCS model.

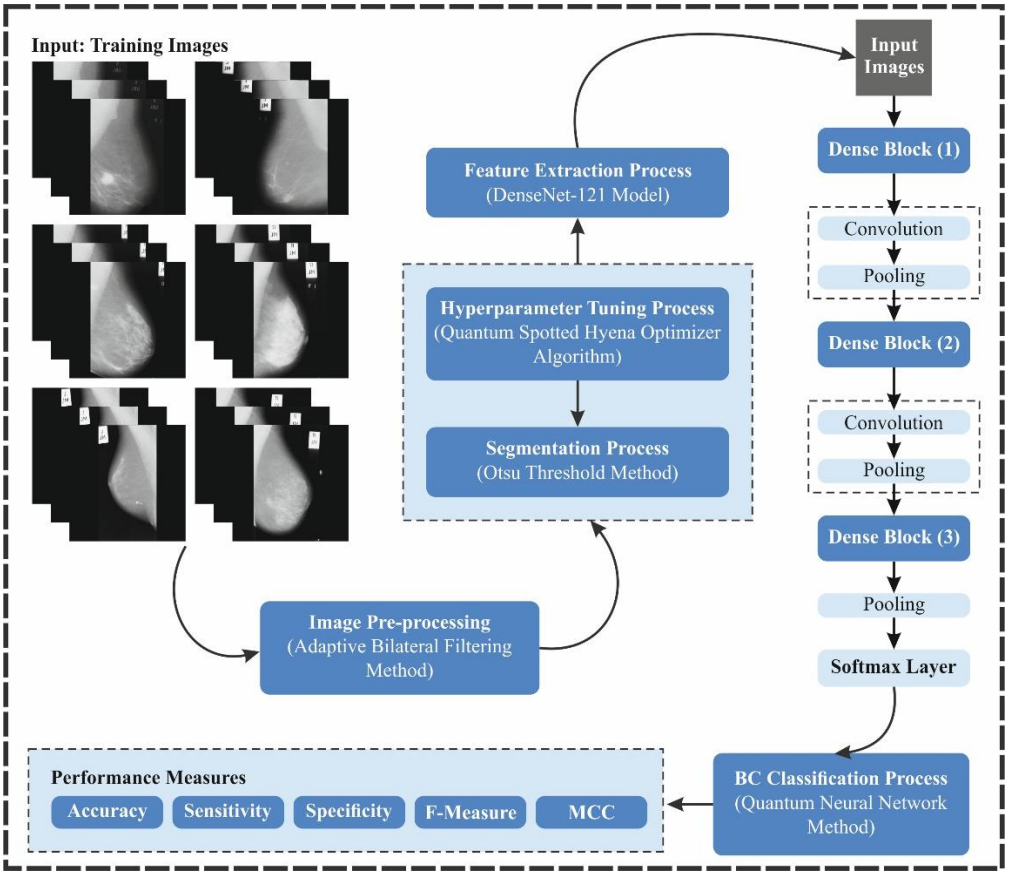

Figure 1. Overall flow of the LQAEDM-IBCS model

A. Image Preprocessing: ABF method

Initially, the image pre-processing stage applies the ABF method to eliminate the unwanted noise in input image data. ABF is a cutting-edge image-processing model that is employed for the detection of edges while maintaining significant details [18]. Unlike typical BF, ABF alters the filter parameters depending upon the local image feature, certifying well noise lessening without concealing edges. It reflects both intensity and spatial differences, making it effective in improving edge structures. The adaptive permits it to manage fluctuating noise levels and textures effectively. This technique is extensively employed in applications such as computer vision, medical imaging, and object detection. By enhancing edges while decreasing noise, ABF enhances edge detection accuracy in complex images.

B. Segmentation Process: Otsu Threshold

Next, the segmentation process is implemented by the Otsu threshold method for edge detection. Otsu threshold segmentation model is a typically applied image segmentation model that is acquired from the least square model principle [19]. It gets a value of threshold T in search within the gray value range of the transmission wire and utilizes the optimal threshold to split the image pixels into dual types: background and wire regions. Formerly, the interclass difference among the background and the traverse areas have been applied as the calculation pattern to estimate the image qualities extraction and segmentation. Nevertheless, the conventional Otsu model may require precisely getting the image gray distribution, leading to segmentation faults. Because of the classical Otsu model,

the best threshold was established by computing the inter-class difference, and the gap amongst the inter-class differences cannot be clear and cannot give the best segmentation effect. Hence, the 2D Otsu threshold segmentation model is presented in a study that can well eliminate noise.

Assume the image size that segmented be $M * N$, the gray value exists $\{0, m\text{-}1\}$, $p(a,b)$ symbolizes pixel point, and $p(a,b) < M$. The average gray value $s(a,b)$ of the neighborhood at pixel point $p(a,b)$ is:

$$s(a,b) = \frac{1}{k*k} \sum_{i=-\frac{k-1}{2}}^{\frac{k-1}{2}} \sum_{i=-\frac{k-1}{2}}^{\frac{k-1}{2}} f\,(m+i, n+j) \tag{1}$$

Here, k characterizes the dimensions of $p(a,b)$ neighborhood searching window. c_{ab} has been applied to characterize the gray values frequencies at coordinates (a,b) within the entire gray range. Its formulation equation is as demonstrated:

$$p(a,b) = \frac{c_{(ab)}}{M*N} \tag{2}$$

The likelihood equation of correlation distribution is as shown in Eq. (3) and (4):

Target area probability:

$$w0 = p(l_0) = \sum_{i=0}^{s} \sum_{j=0}^{t} p\,(a,b) = w_0(s,t) \tag{3}$$

Background area probability:

$$w_1 = p(l_1) = \sum_{i=s+1}^{L-1} \sum_{j=t+1}^{L-1} p\,(a,b) = w_1(s,t) \tag{4}$$

The mean 2D vectors of the dual types of sets are correspondingly stated as:

$$u_0 = (u_{0i}, u_{0j})^T$$

$$= [\sum_{i=0}^{s} \sum_{j=0}^{t} i\,p_{ij}/w_0(s,t), \frac{\sum_{i=0}^{s}\sum_{j=0}^{t} j\,p_{ij}}{w_0(s,t)]^T} \tag{5}$$

$$u_1 = (u_{1i}, u_{1j})^T$$

$$= [\sum_{i=s+1}^{L-1} \sum_{i=t+1}^{L-1} i\,p_{ij}/w_1(s,t), \sum_{i=s+1}^{L-1} \sum_{i=t+1}^{L-1} j\,p_{ij}/w_1(s,t)]^T \tag{6}$$

The average value of incorporated 2D vector is measured by equations (0,1). The particular computation equation is as shown:

$$u_t = (u_{ti}, u_{tj})^T = [\sum_{i=0}^{L-1}\sum_{i=0}^{L-1} i\,p_{ij}, \sum_{i=0}^{L-1}\sum_{i=0}^{L-1} j\,p_{ij}]^T \tag{7}$$

$tr(\mu_B)$ originated from the dispersal matrix has been applied as the distance measurement of the target area and the background area within the segmentation image. The function of the distance measurement amongst the dual types is as shown:

$$tr(\mu_B) = w_0[(u_{0i} - u_{ti})^2 + (u_{0j} - u_{tj})^2] + w_1[(u_{1i} - u_{ti})^2 + \left(u_{1j} - u_{tj}\right)^2] \tag{8}$$

If $tr(\mu_B)$ acquires the maximal value, a 2D vector should be gained, namely, the 2D threshold (s,t) for 2D segmentation of the image:

$$tr\left(\mu_B(S,T)\right) = \max\{tr\left(\mu_B(S,T)\right)\} \tag{9}$$

C. Parameter Tuning: QSHO Algorithm

To improve the segmentation performance, the parameter tuning process is performed through the QSHO algorithm. In QSHO, an original representation, for example, a qubit has been applied for probability-based

representations [20]. A qubit-spotted hyena is a group of qubits. During quantum computing, the probability amplitudes of individual qubits were described by the pairs of numbers (α, β) as:

$$q = \left(\frac{\alpha}{\beta}\right) \tag{10}$$

Whereas α and β fulfill. The qubit hyena is characterized by a group of d qubits as demonstrated:

$$qh = \begin{pmatrix} \alpha_1 & \alpha_2 & \alpha_3 & \cdots & \alpha_d \\ \beta_1 & \beta_2 & \beta_3 & \cdots & \beta_d \end{pmatrix} \tag{11}$$

Here, d refers to size of the optimizer problem to be resolved. A quantum population $Q(t) = \{qh1(t), qh2(t), \ldots, qhN\ (t)\}$ is preserved in QSHO whereas t stands for time (iteration) and N denote the size of the population. The $i\ th$ qubit hyena using d qubits at $t\ th$ time is described as:

$$qhi(t) = \begin{pmatrix} \alpha_{i1}(t) & \alpha_{i2}(t) & \alpha_{i3}(t) & \cdots & \alpha_{id}(t) \\ \beta_{i1}(t) & \beta_{i2}(t) & \beta_{i3}(t) & \cdots & \beta_{id}(t) \end{pmatrix} \tag{12}$$

Each $\alpha_{ij}(t)$ and $\beta_{ij}(t)$ of $qhi(t)$ are randomly initialized by uniform distribution in the interval of (−1, 1) gratifying$\left|\alpha_{ij}(t)\right|^2 + \left|\beta_{ij}(t)\right|^2 = 1$. Having primary initialized $\alpha_{ij}(t)$ and the $\beta_{ij}(t)$ value is calculated as $\beta_{ij}(t) = \sqrt{1 - |\alpha_{ij}(t)|\ 2}$. The population of single angle $\Theta(t) = \{\theta_1(t), \theta_2(t), \theta_3(t), \ldots, \theta_N(t)\}$ was preserved for the quantum population while $\theta_1(t) = \theta_{i1}, \theta_{i2}, \theta_{i3}, \ldots, \theta_{id}$ and $\theta_{ij}(t)$ denote $j\ th$ stage angle for $j\ th$ qubit of $i\ th$ quantum hyena. $\theta_{ij}(t)$ was initialized in the interval of $(0, 2\pi)$. $\theta_{ij}(t)$ has been upgrading over the SHO operator. During this quantum computing method, phase angles in quantum operators should be retained arbitrarily. During this presented QSHO, the phase angles are preserved randomly since QSHO is replicated in conventional computing systems. During QSHO, the quantum location was gained with the usage of quantum rotational gate $U(\cdot)$ as the succeeding:

$$\begin{aligned} q_{ij}^h(t+1) &= \left|U(\theta_{ij}(t+1))q_{ij}^h(t))\right| \\ &= \left|\begin{pmatrix} \cos(\theta_{ij}(t+1)) & -\sin(\theta_{ij}(t+1)) \\ \sin(\theta_{ij}(t+1)) & \cos(\theta_{ij}(t+1)) \end{pmatrix} q_{ij}^h(t)\right| \end{aligned} \tag{13}$$

The location $X_h(t)$ in searching the area of the problems from the quantum location is received as:

$$X_h(t+1) = X_{min} + (X_{max} - X_{min}) \times \left|\alpha_{ij}(t+1)\right| \tag{14}$$

Whereas X_{max} and X_{min} represents the upper and lower limits of the searching region, individually.

$$D_q(t+1) = \left|B.\Theta_p(t) - \Theta_h(t)\right| \tag{15}$$

$$\Theta_h(t+1) = \Theta_p(t) - E.D_q(t) \tag{16}$$

Whereas $D_q(t+1)$ denote the distance among the angles $\Theta_p(t)$ of quantum prey and angle $\Theta_h(t)$ of quantum spotted hyena. The coefficients B and E are upgraded.

The searching behavior was reconsidered as:

$$D_q(t+1) = |B.\Theta_h(t) - \Theta_k(t)| \tag{17}$$

$$\Theta_k(t+1) = \Theta_h(t) - E.D_q(t) \tag{18}$$

Whereas $\Theta_h(t)$ refers to the angles vector of the initial optimal QSH, and $\Theta_k(t)$ denotes the angle vector of another spotted hyena. The cluster or group C_{qh} of L number best solutions are described as shown:

$$C_{qh}(t+1) = \Theta_k(t+1) + \Theta_{k+1}(t+1) + \cdots + \Theta_{k+L}(t+1) \tag{19}$$

Here, L was outlined as:

$$L = count_{nos}\left(\Theta_h, \Theta_{h+1}, \ldots, (\Theta_h + M)\right) \tag{20}$$

Now, M stands for randomly generated vector in [0.5, 1].$count_{nos}(\cdot)$ means similar.

The offensive prey behaviour is reconsidered as:

$$\Theta_h(t+1) = \frac{C_{qh}(t+1)}{L} \tag{21}$$

The pseudocode of QSHO is given in Algorithm 1. During this stage 1 of the model, the parameters h, B, E, N are initialized. Quantum angles and locations of all search agents are primed in stage 2. In stage 3, the locations of searching agents in the search space of the problems are calculated from the quantum location. The fitness of all searching agents is computed in stage 4. In phase 5, the optimal searching agent was discovered and the group of every far best solution is calculated in stage 6. In phases 8-9, the quantum angle of all agents is upgraded. The parameters h, B, E, N are updated in stage 10. The quantum locations of agents are upgraded in stage 12. The location in the search space of the problems from the quantum location is upgraded in stage 13. The fitness of every searching agent is computed in stage 14. $\Theta_h(t)$ and $X_h(t)$ are upgraded in stage 15 and the group $C_{qh}(t)$ is updated in phase 16. The Phases 8-16 are reiterated till maximal iterations $tmax$ is attained.

Algorithm1: Pseudocode of QSHO
Initialization of the parameters h, B, E, N;
Initialization of the population of QSH and quantum angles;
Calculate the location in the search space of the problems from the quantum location utilizing Eq. (14);
Compute the fitness of every searching agent;
$X_h =$ the optimal searching agents;
$C_h =$ the cluster or group of all far best solutions;
whereas $(t < t_{max})$ do
for every search agent do
Updated the quantum angle of the current agent;
Updated $h, B, E,$ and N;
Check if some searching agent surpasses the provided searching region and then adjust it;
Updated the quantum location utilizing Eq. (13);
Calculate the location in the search space for the problems from the quantum location utilizing Eq. (14);
Calculate the fitness of each searching agent;
Updated $\Theta_h(t)$ and $X_h(t)$;
Updated the group $C_{qh}(t)$ w.r.t $\Theta_h(t)$;
$t = t + 1$;
end while
return X_h;

The QSHO originates a fitness function (FF) for attaining an improved performance of segmentation. It defines an optimistic numeral to signify the excellent performance of the candidate solution. Here, the classification rate of error reduction is measured as FF. Its numerical calculation is shown in Eq. (22).

$$fitness(x_i) = ClassifierErrorRate(x_i) = \frac{no.of\ misclassified\ samples}{Total\ no.of\ samples} * 100 \quad (22)$$

D. Feature Extraction: DenseNet-121

Besides, the proposed LQAEDM-IBCS technique designs the DenseNet-121 method for the extraction of feature procedure. DenseNet-121 is a CNN structure with 121 layers proposed [21]. It is well known for its dense connectivity model, every layer associates with each other layer in a feedforward mode for maximum flow of information among layers. The DenseNet structure connects feature mapping learned by dissimilar layers rather than adding them as in conservative CNNs. This increases the flow of information during the network, inspires feature reuse, decreases redundancy, and considerably decreases parameters. Before entering the initial dense block, there are single $7x7$ convolution layer with 64 output channels and a stride of 2, succeeded by a $3x3$ max-pooling layer. The dense blocks feature densely linked convolutional layers, while all layers capture each previous

feature mapping as input. Inside a dense block, layers comprise ReLU activation, batch normalization, a 1x1 convolution (bottleneck layer), and a following 3x3 convolution. Transition layers among dense blocks carried out convolution, batch normalization, and combined 1x1 convolution accompanied by 2x2 average pooling with a compression feature (θ) of 0.5. The last dense block outputs feature maps of changing sizes, resulting in global average pooling before classification into 1000 class labels over a fully connected Softmax layer. Using 7 million parameters and L(L+1)/2 right connections inside every dense block, it denotes its original connectivity and excellent efficacy in different computer vision (CV) tasks.

E. BC Classification Process: QNN Model

Eventually, the QNN method has been deployed for the BC classification process. The QNN is a new idea originating from the connection of quantum computers, ANN, and ML methods [22]. The QNN structure was applied for enormous stages of data processing ability of neural computing that may provide enormous potential in resolving several sequential optimizer problems. The processes of QNN the input data after it is encoded into the relevant qubit condition of the proper quantity of qubits. This qubit condition is then altered for the layer set quantities using parameterized rotational gates with entangling gates, whereas the altered layer of the qubit is established by the predictable profit of the Hamiltonian operator. These results are decoded and converted into functional output data. The NN derived from variational quantum circuits (VQC) implements several tasks in various categories in QNN. In computations, whereas the step counts essential to resolve an issue are calculated in-depth, the complexity-theoretic calculations of accuracy, size, and depth describe individual calculation properties. Accuracy additionally identifies the equipment required to challenge the issue. The technology size frequently considers the problem size. The recommended architecture is a combined intelligent smart system, which utilizes the QNN concept that works completely based on quantum computing. The source of quantum computing refers to qubit $|Q\rangle$, whereas

$$|Q\rangle = x|0\rangle + y|1\rangle \tag{23}$$

q is supposed to signify the variable $|Q\rangle$ in that approach that $|x|^2|y|^2 = 1, x$ and y participate in the type of composite numbers (C). Now, according to the function of Dirac's wave, C denotes the portion of Hilbert's area, x and y mean base amplitudes.

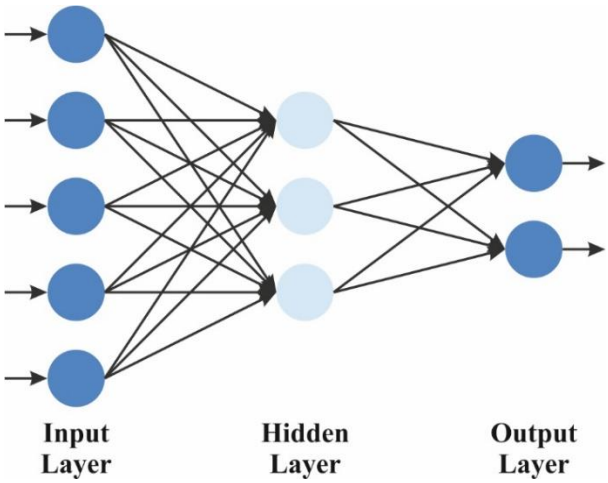

Figure 2. QNN Architecture

A quantum method contains n inputs of the type $|q1\rangle\ i \ldots |qn\rangle\ i$. By utilizing the QNN, the related output $|b\rangle$ established by the rule is made in such cases as shown:

$$\left| b\rangle = A \sum_{j=1}^{n} h\, j \right| qj\rangle \tag{24}$$

Now, A denotes the related activation function applied and h is weight. The similar quantum perceptron output at time s may further be described as demonstrated:

$$\left| b(s)\rangle = A \sum_{j=1}^{n} h\, j(s) \right| qj\rangle \tag{25}$$

Now, weight (h) and related activation function (A) are applied. The succeeding type is additionally used for the quantum perceptron output at time s:

$$hj(s+1 = hj(s) + \mu(|\bar{b}\rangle - |b(s))\rangle\langle qj| \quad (26)$$

$\overline{b}$ should be the predictable result. Fig. 2 represents the infrastructure of QNN.

4. Performance Validation

The simulation validation of the LQAEDM-IBCS approach is inspected under the mini-MIAS Mammography dataset [23]. This dataset consists of 319 instances under three class labels such as normal, benign, and malignant as depicted in Table 1. Fig. 3 signifies the sample images.

Table 1: Details of the dataset

Class Labels	No. of Instances
Normal	207
Benign	63
Malignant	49
Total Instances	319

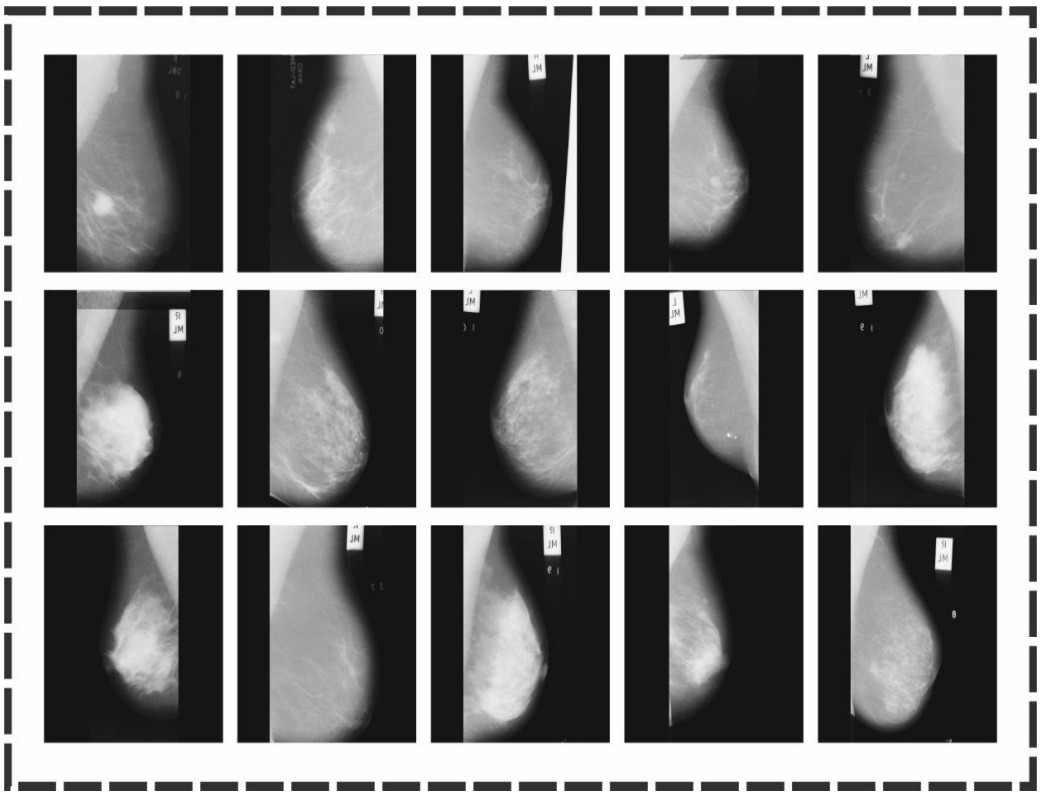

Figure 3. Sample Images

Fig. 4 displays the classifier analysis of the LQAEDM-IBCS technique. Figs. 4a-4b displays the confusion matrices through precise classification and identification of all classes below 70%TRAPHA and 30%TESPHA. Fig. 4c exemplifies the PR examination, which notified higher outcomes through all class labels. At last, Fig. 4d represents the ROC inspection, signifying proficient outcomes through high ROC values for different classes.

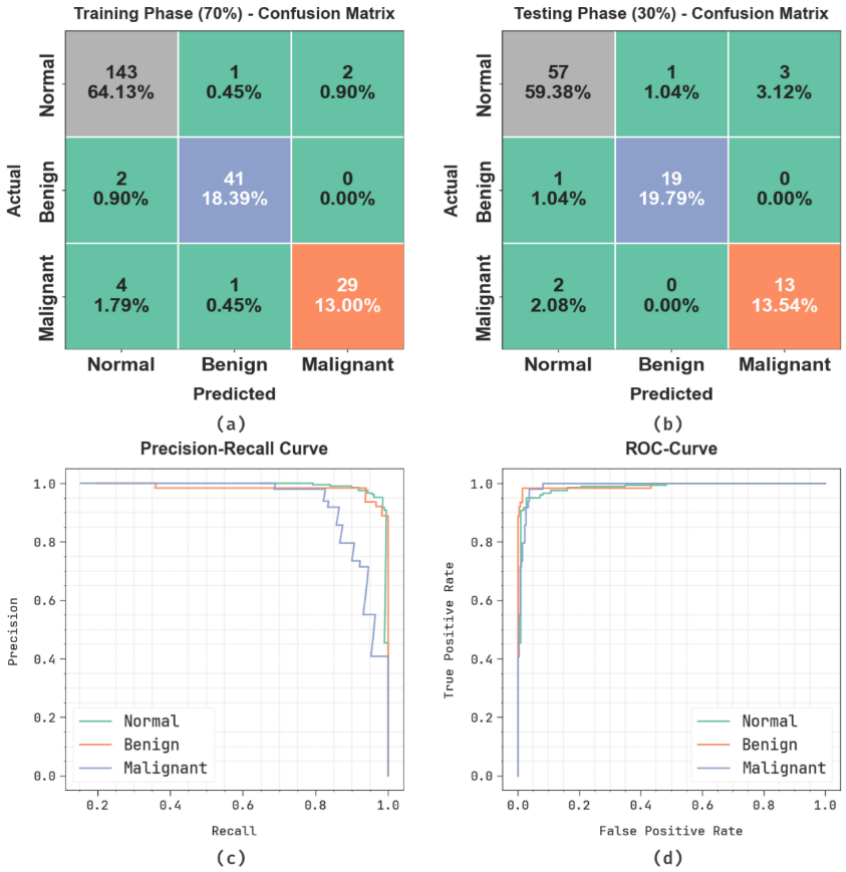

Figure 4. Classifier outcome of (a-b) 70% and 30% confusion matrices and (c-d) curves of PR and ROC

Table 2 and Fig. 5 study the BC edge detection of the LQAEDM-IBCS method under 70%TRAPHA and 30%TESPHA. The performances stated that the LQAEDM-IBCS model suitably classified all the samples. Using 70%TRAPHA, the LQAEDM-IBCS algorithm provides typical $accu_y$ of 97.01%, $sens_y$ of 92.86%, $spec_y$ of 96.68%, $F_{Measure}$ of 93.84%, and MCC of 90.93%. Furthermore, according to 30%TESPHA, the LQAEDM-IBCS model delivers typical $accu_y$ of 95.14%, $sens_y$ of 91.70%, $spec_y$ of 95.47%, $F_{Measure}$ of 91.03%, and MCC of 86.30%.

Table 2: BC edge detection of LQAEDM-IBCS model under 70%TRAPHA and 30%TESPHA

Class	$Accu_y$	$Sens_y$	$Spec_y$	$F_{Measure}$	MCC
TRAPHA (70%)					
Normal	95.96	97.95	92.21	96.95	91.03
Benign	98.21	95.35	98.89	95.35	94.24
Malignant	96.86	85.29	98.94	89.23	87.53
Average	97.01	92.86	96.68	93.84	90.93
TESPHA (30%)					
Normal	92.71	93.44	91.43	94.21	84.38
Benign	97.92	95.00	98.68	95.00	93.68
Malignant	94.79	86.67	96.30	83.87	80.83
Average	95.14	91.70	95.47	91.03	86.30

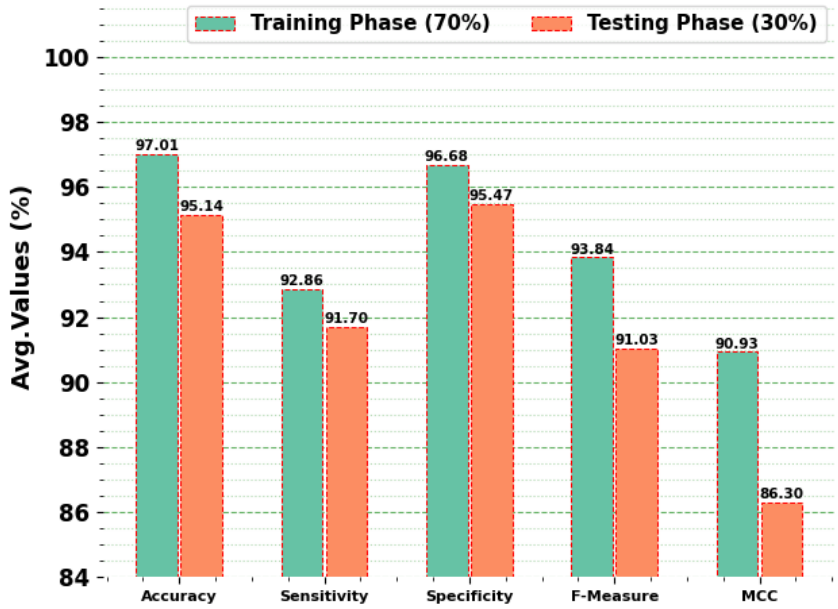

Figure 5. Average of LQAEDM-IBCS model under 70%TRAPHA and 30%TESPHA

In Fig. 6, the TRAN $accu_y$ and VALN $accu_y$ performances of the LQAEDM-IBCS technique are illustrated. The values of $accu_y$ are computed across a time of 0-50 epochs. The figure underscored that the TRAN and VALN$accu_y$ values express a growing propensity, indicating the proficiency of the LQAEDM-IBCS method using enhanced outcomes through multiple repetitions. In addition, the TRAN and VALN $accu_y$ ruins nearer through the epochs, notifying decreased overfitting and presenting superior performance of the LQAEDM-IBCS system, which guarantees reliable calculation on hidden samples.

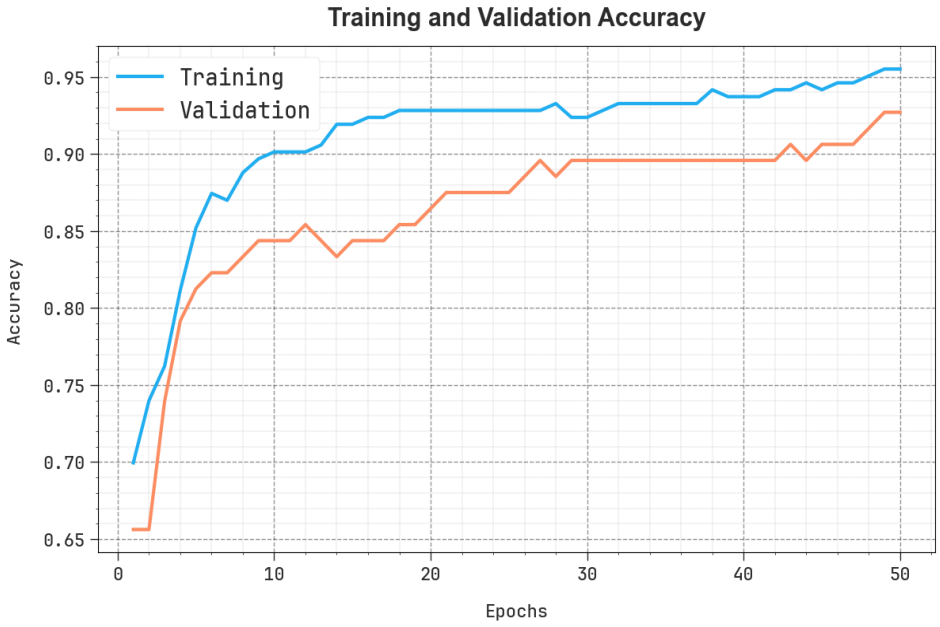

Figure 6. $Accu_y$ Curve of LQAEDM-IBCS model

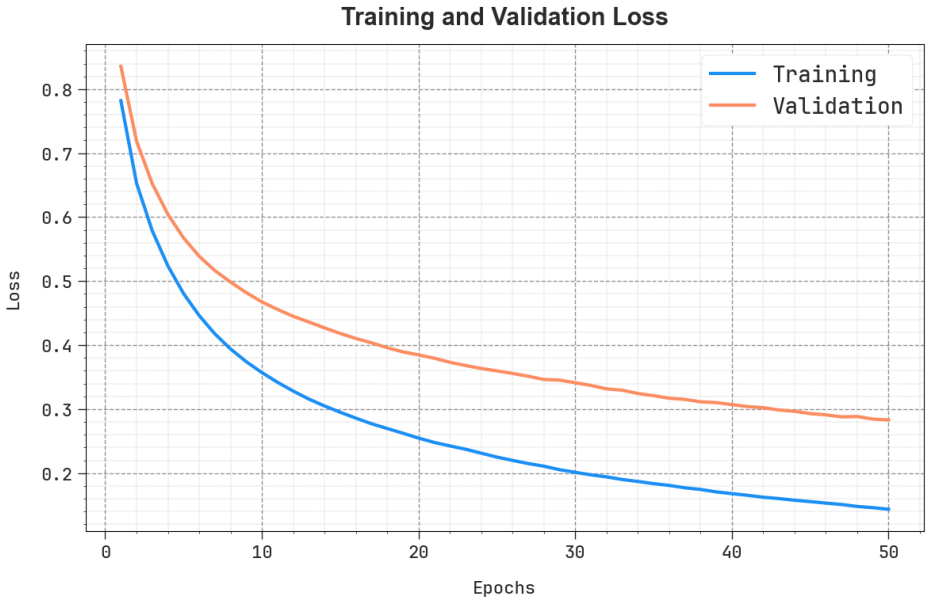

Figure 7. Loss curve of LQAEDM-IBCS model

In Fig. 7, the TRANLOS and VALNLOS graph of the LQAEDM-IBCS technique is depicted. The values of loss are computed through a period of 0-50 epochs. It is indicated that the TRANLOS and VALNLOS values demonstrate a declining trend, which indicates the competency of the LQAEDM-IBCS method in equalizing an equilibrium between data fitting and generalization. The consecutive dilution in values of loss also assurances the maximum performance of the LQAEDM-IBCS algorithm and tunes the calculation results after a while.

Table 3 provides the comparative analysis of the LQAEDM-IBCS model with existing classifiers under various metrics [24].

Table 3: Comparative analysis of the LQAEDM-IBCS model with existing classifiers

Methods	$Accu_y$	$Sens_y$	$Spec_y$	$F_{Measure}$
DL-CADSBM	93.07	91.06	95.65	90.52
MCNN-MIC	82.06	90.19	95.37	90.80
CMIM-CNN	83.06	90.07	95.08	90.84
ResNet-ResNet	92.08	87.07	89.07	90.37
ResNet-VGG	94.08	88.05	92.06	89.12
BMCS-DL ELDM	95.07	90.07	95.08	89.90
BMCA-AOADL	96.55	90.76	95.44	92.69
LQAEDM-IBCS	97.01	92.86	96.68	93.84

Fig. 8 examines$accu_y$, and $F_{Measure}$ solutions of the LQAEDM-IBCS model with existing methodologies. According to $accu_y$, the LQAEDM-IBCS system has a maximum $accu_y$ of 97.01% whereas the DL-CADSBM, MCNN-MIC, CMIM-CNN, ResNet-ResNet, ResNet-VGG, BMCS-DL ELDM, and BMCA-AOADL algorithm have attained minimal $accu_y$ of 93.07%, 82.06%, 83.06%, 92.08%, 94.08%, 95.07%, and 96.55%, correspondingly. Additionally, on $F_{Measure}$, the LQAEDM-IBCS model has superior $F_{Measure}$ of 93.84% whereas the DL-CADSBM, MCNN-MIC, CMIM-CNN, ResNet-ResNet, ResNet-VGG, BMCS-DL ELDM, and BMCA-AOADL techniques have gained diminished $F_{Measure}$ of 90.52%, 90.80%, 90.84%, 90.37%, 89.12%, 89.90%, and 92.69%, respectively.

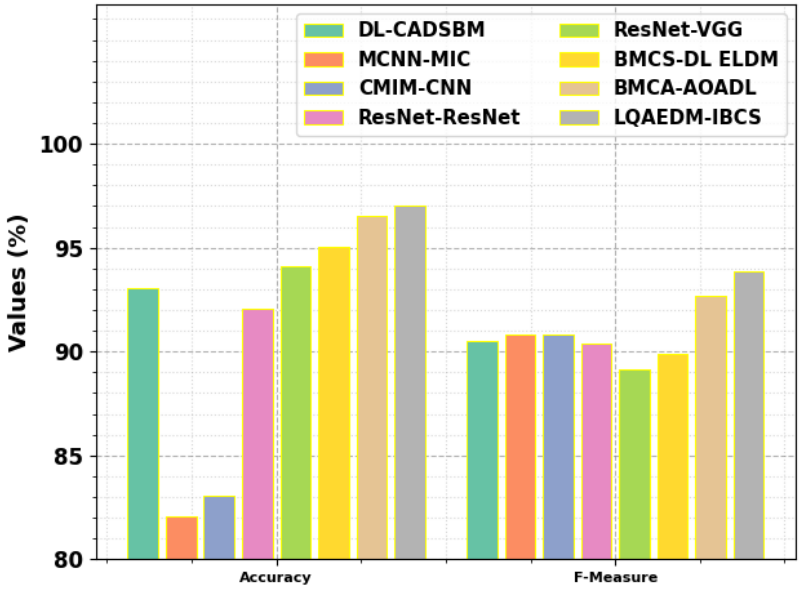

Figure 8. $Accu_y$, and $F_{Measure}$ outcome of the LQAEDM-IBCS method with existing models

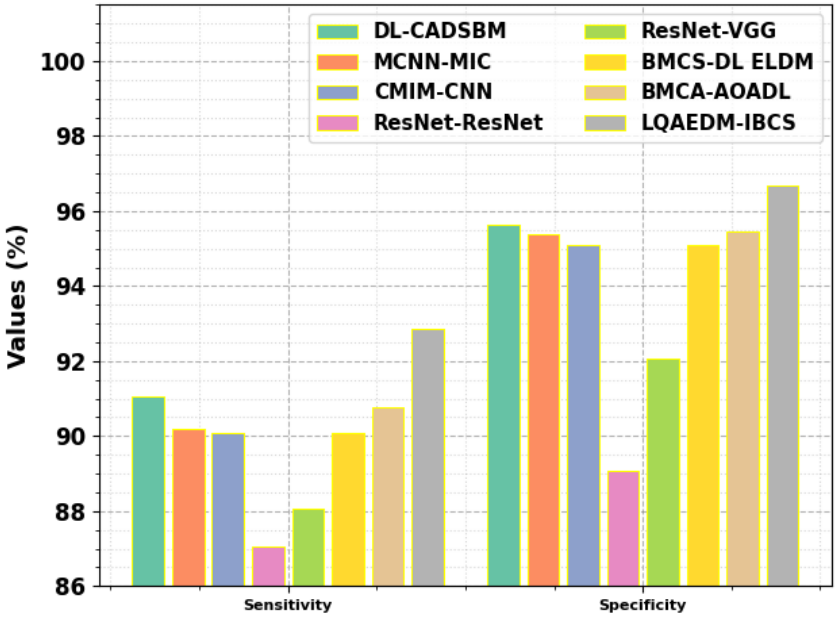

Figure 9. $Sens_y$ And $Spec_y$ outcome of the LQAEDM-IBCS method with existing models

Fig. 9 studies the $sens_y$, and $spec_y$ analysis of the LQAEDM-IBCS algorithm with existing techniques. With$sens_y$, the LQAEDM-IBCS method has increased $sens_y$ of 92.86% whereas the DL-CADSBM, MCNN-MIC, CMIM-CNN, ResNet-ResNet, ResNet-VGG, BMCS-DL ELDM, and BMCA-AOADL methodologies have reached minimal $sens_y$ of 91.06%, 90.19%, 90.07%, 87.07%, 88.05%, 90.07%, and 90.76%, correspondingly. Afterward, using $spec_y$, the LQAEDM-IBCS model has increased $spec_y$ of 96.68% whereas the DL-CADSBM, MCNN-MIC, CMIM-CNN, ResNet-ResNet, ResNet-VGG, BMCS-DL ELDM, and BMCA-AOADL algorithms have accomplished lower $spec_y$ of 95.65%, 95.37%, 95.08%, 89.07%, 92.06%, 95.08%, and 95.44%, respectively.

5. Conclusion

In this study, we design an LQAEDM-IBCS model. The main intention of the LQAEDM-IBCS is to provide a correct and effective performance for the detection and segmentation process of BC utilizing advanced algorithms. Initially, the image pre-processing stage applies the ABF method to eliminate the unwanted noise in input image data. Next, the segmentation process is implemented by the Otsu threshold method for edge detection. To improve

the segmentation performance, the parameter tuning process is performed through the QSHO algorithm. Besides, the proposed LQAEDM-IBCS technique designs the DenseNet-121 method for the extraction of feature procedure. Eventually, the QNN method has been deployed for the BC classification process. The simulating validation of the LQAEDM-IBCS system is verified on a benchmark image database and the outcomes are dignified under numerous measures. The experimental outcome emphasized the enlargement of the LQAEDM-IBCS approach in the BC diagnosis process.

Funding: "This research received no external funding"

Conflicts of Interest: "The authors declare no conflict of interest."

References

[1] A. Tariq Jamal, A. Ben Ishak, and S. Abdel-Khalek, "Tumor edge detection in mammography images using quantum and machine learning approaches," *Neural Comput. Appl.*, vol. 33, no. 13, pp. 7773–7784, 2021.

[2] S. Dey, R. Roychoudhury, S. Malakar, and R. Sarkar, "Screening of breast cancer from thermogram images by edge detection aided deep transfer learning model," *Multimedia Tools Appl.*, vol. 81, no. 7, pp. 9331–9349, 2022.

[3] Z. Wang et al., "Breast cancer detection using extreme learning machine based on feature fusion with CNN deep features," *IEEE Access*, vol. 7, pp. 105146–105158, 2019.

[4] G. Guo and N. Razmjooy, "A new interval differential equation for edge detection and determining breast cancer regions in mammography images," *Syst. Sci. Control Eng.*, vol. 7, no. 1, pp. 346–356, 2019.

[5] G. Murtaza et al., "Deep learning-based breast cancer classification through medical imaging modalities: state of the art and research challenges," *Artif. Intell. Rev.*, vol. 53, pp. 1655–1720, 2020.

[6] D. Q. Zeebaree, H. Haron, A. M. Abdulazeez, and D. A. Zebari, "Machine learning and region growing for breast cancer segmentation," in *Proc. Int. Conf. Adv. Sci. Eng. (ICOASE)*, 2019, pp. 88–93.

[7] S. Chaudhury et al., "[Retracted] Effective image processing and segmentation-based machine learning techniques for diagnosis of breast cancer," *Comput. Math. Methods Med.*, vol. 2022, no. 1, p. 6841334, 2022.

[8] H. Zerouaoui and A. Idri, "Reviewing machine learning and image processing based decision-making systems for breast cancer imaging," *J. Med. Syst.*, vol. 45, no. 1, p. 8, 2021.

[9] Y. Xu et al., "Medical breast ultrasound image segmentation by machine learning," *Ultrasonics*, vol. 91, pp. 1–9, 2019.

[10] S. Dey, R. Roychoudhury, S. Malakar, and R. Sarkar, "Screening of breast cancer from thermogram images by edge detection aided deep transfer learning model," *Multimedia Tools Appl.*, vol. 81, no. 7, pp. 9331–9349, 2022.

[11] D. Youssef, H. Atef, S. Gamal, J. El-Azab, and T. Ismail, "Early breast cancer prediction using thermal images and hybrid feature extraction based system," *IEEE Access*, 2025.

[12] M. Olota et al., "Modified anisotropic diffusion and level-set segmentation for breast cancer," *Multimedia Tools Appl.*, vol. 83, no. 5, pp. 13503–13525, 2024.

[13] P. Ghafariasl, M. Zeinalnezhad, and S. Chang, "Fine-tuning pre-trained networks with emphasis on image segmentation: A multi-network approach for enhanced breast cancer detection," *Eng. Appl. Artif. Intell.*, vol. 139, p. 109666, 2025.

[14] G. Murtaza et al., "Deep learning-based breast cancer classification through medical imaging modalities: state of the art and research challenges," *Artif. Intell. Rev.*, vol. 53, pp. 1655–1720, 2020.

[15] A. Bilal et al., "A quantum-optimized approach for breast cancer detection using SqueezeNet-SVM," *Sci. Rep.*, vol. 15, no. 1, p. 3254, 2025.

[16] L. Singh and A. Alam, “An efficient hybrid methodology for early detection of breast cancer in digital mammograms,” *J. Ambient Intell. Humanized Comput.*, vol. 15, no. 1, pp. 337–360, 2024.

[17] F. Taheri and K. Rahbar, “Improving breast cancer classification in fine-grain ultrasound images through feature discrimination and a transfer learning approach,” *Biomed. Signal Process. Control*, vol. 106, p. 107690, 2025.

[18] W. Guo, P. Lu, X. Peng, and Z. Zhao, “Learnable adaptive bilateral filter for improved generalization in single image super-resolution,” *Pattern Recognit.*, p. 111396, 2025.

[19] W. Qi, Z. Yuan, L. Tan, and Z. Wang, “Research on detection of new energy power line based on computer vision,” *Int. J. Low-Carbon Technol.*, vol. 20, pp. 480–487, 2025.

[20] T. Si et al., “QSHO: Quantum spotted hyena optimizer for global optimization,” *Artif. Intell. Rev.*, vol. 58, no. 3, p. 71, 2025.

[21] D. M. Farid, P. K. Das, M. Islam, and E. Sina, “Bangladeshi vehicle classification and detection using deep convolutional neural networks with transfer learning,” *IEEE Access*, 2025.

[22] H. Kadry, A. Farouk, E. A. Zanaty, and O. Reyad, “Intrusion detection model using optimized quantum neural network and elliptical curve cryptography for data security,” *Alexandria Eng. J.*, vol. 71, pp. 491–500, 2023.

[23] MIAS database. [Online]. Available: http://peipa.essex.ac.uk/info/mias.html

[24] M. Basheri, “Intelligent breast mass classification approach using Archimedes optimization algorithm with deep learning on digital mammograms,” *Biomimetics*, vol. 8, no. 6, p. 463, 2023.